Heat Exchange Effectiveness and Pressure Drop for Air Flow Through Perforated Plates With and Without Crosswind

C. F. Kutscher
National Renewable Energy Laboratory,
1617 Cole Boulevard,
Golden, CO 80401
Mem. ASME

Low-porosity perforated plates are being used as absorbers for heating ambient air in a new type of unglazed solar collector. This paper investigates the convective heat transfer effectiveness for low-speed air flow through thin, isothermal perforated plates with and without a crosswind on the upstream face. The objective of this work is to provide information that will allow designers to optimize hole size and spacing. In order to obtain performance data, a wind tunnel and small lamp array were designed and built. Experimental data were taken for a range of plate porosities from 0.1 to 5 percent, hole Reynolds numbers from 100 to 2000, and wind speeds from 0 to 4 m/s. Correlations were developed for heat exchange effectiveness and also for pressure drop. Infrared thermography was used to visualize the heat transfer taking place at the surface.

1.0 Introduction

Perforated plates have been used for multiple-plate heat exchangers, film cooling (e.g., of turbine blades), and most recently in a new type of solar collector used to heat ambient air (Kutscher et al., 1993). Despite numerous applications, few studies have been done on the heat transfer coefficients for air flowing through these plates. Sparrow and Ortiz (1982) used the naphthalene sublimation technique to deduce heat transfer coefficients on the upstream face for air flowing normal to perforated plates. They tested two plates containing holes arranged in a staggered array, one with 14 percent open area and the other with 22 percent open area. A hole Reynolds number range of 2000 to 20,000 was covered.

As part of a series of studies related to film cooling applications, Andrews and Bazdidi-Tehrani (1989) conducted transient cool-down tests on a wide range of 6.35-mm-thick perforated plates containing square arrays of holes with different hole diameters and pitches. They obtained a correlation for the overall Nusselt number for normal flow as follows:

$$\mathrm{Nu}_D = 2.44\left(\frac{P}{D}\right)^{-1.43} \mathrm{Re}_D^{0.57}\mathrm{Pr}^{0.33} \tag{1}$$

which is said to cover $500 < \mathrm{Re}_D \leq 43{,}000$, $1.9 < P/D < 22$, and $0.8 < t/D < 9.9$. The range of suction mass flow rates covered was from 0.1 to 1.7 kg/m^2-s.

Transpired solar collectors consist of an unglazed black perforated plate through which outside air is drawn by a fan (see Fig. 1). The air is preheated as it passes through the irradiated plate and is subsequently used for applications such as building ventilation air or crop drying. A typical range of mass suction flow rates is $G = 0.01$ to 0.05 kg/m^2-s. (As shown by Kutscher et al., 1993, at an incident radiation level of 700 W/m^2, these suction rates would correspond to an air temperature rise of roughly 36°C at the low flow rate and 12°C at the high flow rate.) In order to predict the efficiency of this type of collector, one must know the heat exchange effectiveness for the transpired air stream. The heat transferred from the plate to the suction air stream and the heat exchange effectiveness can be written in terms of an overall heat transfer coefficient based on the difference between plate and inlet air temperatures or one based on the logarithmic mean temperature difference as follows. To make the distinction between these two definitions clear, this paper will call the former h (consistent with the papers by Sparrow and Ortiz and Andrews et al.) and the latter U (consistent with most heat exchanger texts). Thus the heat transferred and the heat exchange effectiveness can be written as follows:

$$Q = hA(T_s - T_{\mathrm{amb}}) = UA\,\frac{T_o - T_{\mathrm{amb}}}{\ln\dfrac{T_s - T_{\mathrm{amb}}}{T_s - T_o}} \tag{2}$$

$$\epsilon_{HX} = \frac{T_o - T_{\mathrm{amb}}}{T_s - T_{\mathrm{amb}}} = \frac{hA}{\dot{m}C_p} = 1 - e^{-\frac{UA}{\dot{m}C_p}} \tag{3}$$

Note that physically the heat exchange effectiveness is equal to the ratio of the heat transferred to the air stream to the maximum possible heat transfer (i.e., if the outlet air were

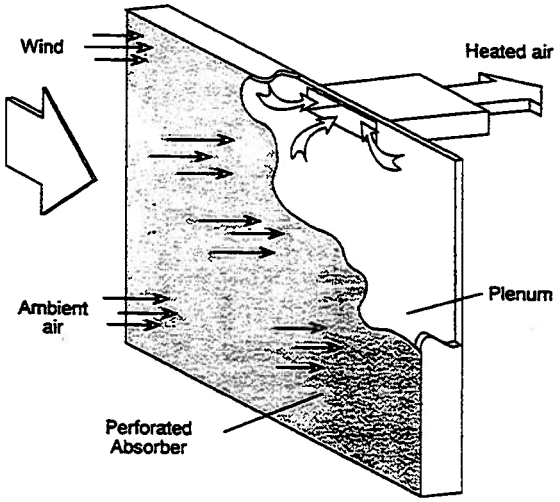

Fig. 1 Unglazed transpired solar collector oriented vertically for building ventilation preheat

Contributed by the Heat Transfer Division for publication in the JOURNAL OF HEAT TRANSFER. Manuscript received by the Heat Transfer Division April 1993; revision received July 1993. Keywords: Forced Convection, Heat Exchangers, Solar Energy. Associate Technical Editor: W. A. Fiveland.

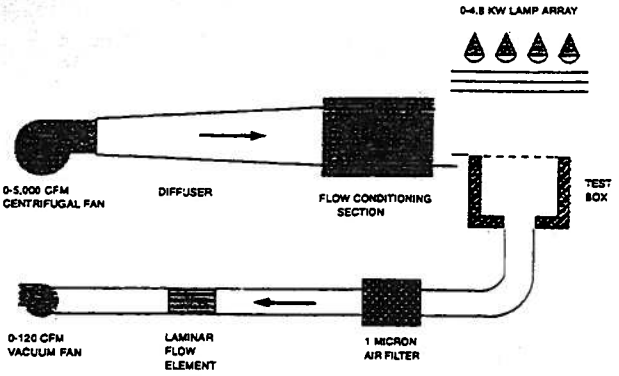

Fig. 2 Transpired collector test facility showing wind tunnel, test loop, and lamp array

heated to the plate surface temperature). Andrews and Bazdidi-Tehrani (1989) developed a correlation for Nusselt number based on h. In their correlation, h varies as the approach velocity raised to a power between 0 and 1. (The same is true for the work of Sparrow and Ortiz on front-surface-only heat transfer. They found that h for the front surface was proportional to $\mathrm{Re}_D^{0.476}$.) It readily can be seen that with such correlations, as suction velocity approaches zero, the heat exchange effectiveness is unbounded.

This was not necessarily a problem for their work, as their suction flow rates were high enough that the heat exchange effectiveness was always less than one. For the low flow rates used for transpired collectors, however, one must ensure that the correlation obtained yields physically realistic heat exchange effectiveness values. Although correlations can be developed for heat transfer coefficients based on either $(T_s - T_{amb})$ or the log mean temperature difference, only the latter (U) can be correlated as a simple power law in mass flow rate. The purpose of this study was to develop a useful heat transfer correlation for flow through perforated plates under the conditions used for transpired collectors. These conditions are low porosity (typically less than 2 percent), low suction flow rates (0.01 to 0.05 kg/m^{2}s), staggered hole arrays, a thin aluminum plate (0.794 mm or 1/32 in.), and a crosswind on the upstream surface. (Some heat transfer enhancement can also occur on the back surface due to the flow in a plenum, but this is strongly dependent on the plenum used, and experimental tests at NREL have shown that this is a small effect.) Further details of the work presented here, including analytical and numerical modeling are contained in Kutscher (1992).

2.0 Experimental Apparatus

An overall schematic of the experimental setup is shown in Fig. 2. Rectangular perforated aluminum test plates of dimensions 30 cm × 50 cm were tested. The test plate dimensions were selected to allow sufficient length that measurements for crosswind tests could be taken in the region of asymptotic boundary layer thickness and sufficient width to allow plate centerline measurements to be undisturbed by edge effects. The plates were mounted atop an insulated and sealed plywood box. An additional perforated plate was used inside the box to ensure uniform flow through the test plate. Air exited the box through a 5.1 cm (2 in.) CPVC pipe, which penetrated the center of the floor of the box.

The top lid was essentially a frame that held the test absorber. The absorber to be tested was mounted on a series of plastic pins protruding from the inner edge of the frame that provided minimal conduction paths between the absorber and the frame. Tape was used to cover the gap between the metal absorber and the frame to prevent leakage around the edge of the absorber. Both the top and a long side of the box were removable for instrumentation access.

Suction through the box was provided by an Ametek 0-120 CFM vacuum fan driven by a universal AC-DC motor, and the motor speed was controlled by a 10 amp variable transformer. A combination of sliding gate dampers and a room air inlet pipe upstream of the fan (but downstream of the flow measuring section) was used to maintain operation at stable operating points for the suction fan and the transformer.

Electric resistance and radiative heating were considered as possible means for providing uniform heat flux to the test plates. Radiative heating was selected because its flux uniformity was not affected by the presence of holes, it lent itself well to testing a wide range of hole geometries, and it worked well with the aluminum plates generally used for solar collector applications. After testing a number of candidate lamps, GE R-40 300-watt flood lamps were chosen because they provided reasonably uniform illumination without local hot spots.

Obtaining uniform flux with an array of such lamps is not a trivial matter. A computer program was written to perform simulated tests of various lamp configurations. For simplicity, all lamps were aimed normal to the plane of the test absorber, which was located approximately 1 m away. The final array

Nomenclature

A = area of unit cell on plate less hole area, m^2
A' = area of unit cell on plate, m^2
c_p = air specific heat at constant pressure, J/kg-K
D = hole diameter, m
G = suction mass flow rate based on unit area A', kg/m^2-s
h = convective heat transfer coefficient based on $(T_s - T_{amb})$ and area A, W/m^2-K
k = air thermal conductivity, W/m^2-K
L_s = starting length to establish asymptotic boundary layer, m
$\dot{m}$ = suction mass flow rate, kg/s
NTU = $UA/\dot{m}c_p$ = number of transfer units
NTS = plate orientation with narrow transverse (i.e., in the direction normal to the wind) spacing of holes
Nu_x = Ux/k or hx/k = Nusselt number
P = hole pitch, i.e., distance between center of hole and center of next closest hole, m
Pr = ν/α = Prandtl number
Re_x = vx/ν = Reynolds number, where v is relevant velocity scale
Q = heat transferred from plate to air stream, W
t = plate thickness, m
T_{amb} = ambient temperature = T_∞, K
T_o = air outlet temperature, K
T_s = plate surface temperature, K
U = convective heat transfer coefficient based on log mean temperature difference and area A, W/m^2-K
U_∞ = free-stream velocity, wind speed, m/s
V = average suction face velocity, m/s
WTS = plate orientation with wide transverse (i.e., in the direction normal to the wind) spacing of holes
ΔP = pressure drop, Pa
α = air thermal diffusivity, m^2/s
δ = velocity boundary layer thickness, m
ϵ_{HX} = absorber heat exchange effectiveness
ζ = $(1/2)\rho V^2$ = nondimensional pressure drop
μ = air viscosity, kg/m-s
ν = air kinematic viscosity, m^2/s
σ = plate porosity, or open area fraction
ρ = air density, kg/m^3

configuration contained 16 lamps with a large open area in the middle of the array that eliminated a hot spot in the middle of the absorber that otherwise would be caused by the overlap there of the tails of all the lamp distributions. This configuration "wasted" some lamp energy compared with a scheme utilizing individual lamp tilting, but resulted in excellent flux uniformity of better than ±2 percent (measured by a Kipp & Zonen CM-11 pyranometer) with modest power requirements. The lamps were divided into two separate subarrays of 8 lamps each allowing the use of two 30-amp circuits. Each subarray was controlled by a separate 0-140 V output variable transformer, and these were kept at identical power settings by using two matched digital voltmeters. The transformers not only allowed the lamps to be adjusted to lower settings but also allowed much higher flux levels (exceeding 1200 W/m^2) by applying overvoltage to the 120 V lamps.

To provide a crosswind, a low-speed wind tunnel was built. An open circuit blow-through design was selected in order to provide easy access to the test section and to allow unobstructed viewing with an Inframetrics infrared camera. Because of the large amount of flow conditioning needed downstream of a fan, a high-head 2.36 m^3/s (5000 CFM) centrifugal unit was used in conjunction with considerable flow conditioning. A Fincor adjustable speed drive was used to allow the fan to be set from 0 to 1670 rpm. The flow conditioning consisted of a plastic honeycomb with one screen upstream of the honeycomb and seven screens downstream. The screen frames and honeycomb edge were seated into grooves routed into the inner styrofoam walls of the flow conditioning section.

The cross section of the flow conditioning section and tunnel exit was 0.362 m × 0.64 m (14.25 in. × 25 in.). This size allowed the test plate to be immersed in the inviscid core of undisturbed air exiting the tunnel. Tests were done with plates in both horizontal (face-up) and vertical orientations. To switch from one orientation to another, the entire assembly including test box, lamp array, and wind tunnel was rotated 90 deg. To remove boundary layer air along the edge (either floor or side) of the wind tunnel aligned with the test plate, a sharp leading edge was installed upstream of the test plate and extending 17 cm from the beginning of suction. Orginally, the boundary layer air was allowed to exit under the leading edge passively. It was found later that more precise splitting of streamlines could be obtained by adding active suction via a small fan and speed controller. Flow visualization was done via a smoke wire consisting of 10-mil constantan (from a 30 gage copper-constantan thermocouple wire), coated with oil, and heated with approximately 10 volts AC. Figure 3 shows smoke wire results indicating the effect of the boundary layer removal and the overall character of the flow.

3.0 Instrumentation

Absolute temperatures were measured with YSI 10,000 ohm thermistors. Temperature differences were measured both with the YSI thermistors and with special calibration type T (copper-constantan) thermocouples arranged in a thermopile circuit with voltages converted to temperature differences via a Newton–Raphson inversion routine in the software.

For surface temperature readings, sensors were glued to the underside of the plate with a high thermal conductivity epoxy, and lead wires were glued along the plate for a distance of 5 cm. It is important to note that for the aluminum plates tested, there was no measurable difference in temperature from the centerpoint between holes to the edge of a hole. This was verified by both multiple surface probes and by infrared thermography of the surface as well as by numerical simulations of the problem (to be reported in a separate paper). The ambient air temperature reading was taken several centimeters above the plate with sensors mounted in a double radiation shielded probe with both shields highly aspirated. Temperatures inside the test box were taken with an array of unshielded 30 gage type T thermocouples and with a thermistor mounted in a specially designed radiation shielded, low-aspiration-rate porous probe.

Suction flow rate was read with a calibrated Meriam laminar flow element with the pressure drop across the element measured by a calibrated MKS pressure transducer. This flow measuring device allowed a range of 10 to 1 on suction rates with a ±1 percent of reading accuracy. Wind tunnel velocity was determined by taking pitot tube measurements at speeds from 3 to 10 m/s and correlating these to fan rpm (measured by an optical tachometer). A plot of fan rpm versus wind tunnel speed was found to be extremely linear with no offset at zero, and so fan rpm was used to determine wind speed even at speeds less than 3 m/s. The test plate pressure drop was measured with a Dwyer point gage manometer having a range of 0-498 Pa (0–2 in. water) and readable to 2.29 Pa (0.001 in. water).

Data acquisition was done with an HP-75000 B-frame VXI bus data acquisition system with an internal HP-1326 5-1/2 digit digital voltmeter and several multiplexer/thermocouple cards. The data acquisition unit was controlled by an IBM PC-AT programmed in HT-Basic.

4.0 Normal Flow Effectiveness Results

Three different methods for determining heat exchange effectiveness were considered: transient cool-down (similar to the method used by Andrews et al.), energy balance method, and direct ΔT measurement. In the transient method, the plate is heated above ambient by the lamp array, and then the lamp radiation is blocked by a shield. The heat transfer coefficient can be determined from the slope of the temperature versus time curve as the plate cools down. In the energy balance method, the net radiation on the plate is measured, and this is assumed equal to the energy in the airstream.

In the direct temperature measurement method, the effectiveness is simply found from the definition:

$$\epsilon_{HX}=\frac{T_o-T_{amb}}{T_s-T_{amb}} \tag{4}$$

where T_o is the outlet air temperature in K.

An uncertainty analysis was done in accordance with ANSI/ASME PTC 19.1–1985. The uncertainties in temperature measurements (including installation effects) were estimated to be as follows: ±0.3 K for T_s, ±0.4 K for T_o, and ±0.5 K for T_{amb}. Figure 4 shows a comparison of the estimated experimental uncertainty for all three methods using an effectiveness model based on the final data correlation for zero wind results. (An approximate model used for initial assessment of the three experimental methods yielded similar relative results.) Note that the direct method has good accuracy at high effectiveness values. This is because ΔT's are high, and so the impact of uncertainties in the temperature measurements is low. At low values of effectiveness, the direct method is poor, although accuracy can be improved by turning the lamp array voltage up and reaching flux values of 1200 W/m^2 or more. (The curves in Fig. 4 are based on a flux of 800 W/m^2.)

For solar collector applications, high effectiveness values are mostly of interest, and the plates tested ranged in effectiveness from about 0.40 to about 0.90. The direct temperature measurement method has reasonably good accuracy over this region, and it has the additional advantage that it directly yields the quantity of interest without requiring any conversion. Because of these reasons, as well as the excellent repeatability found in the lab tests, it was chosen as the prime measurement technique, and the results reported here were obtained by this method.

To determine parameter sensitivities efficiently, the experimental work began with a full factorial test of 16 runs covering

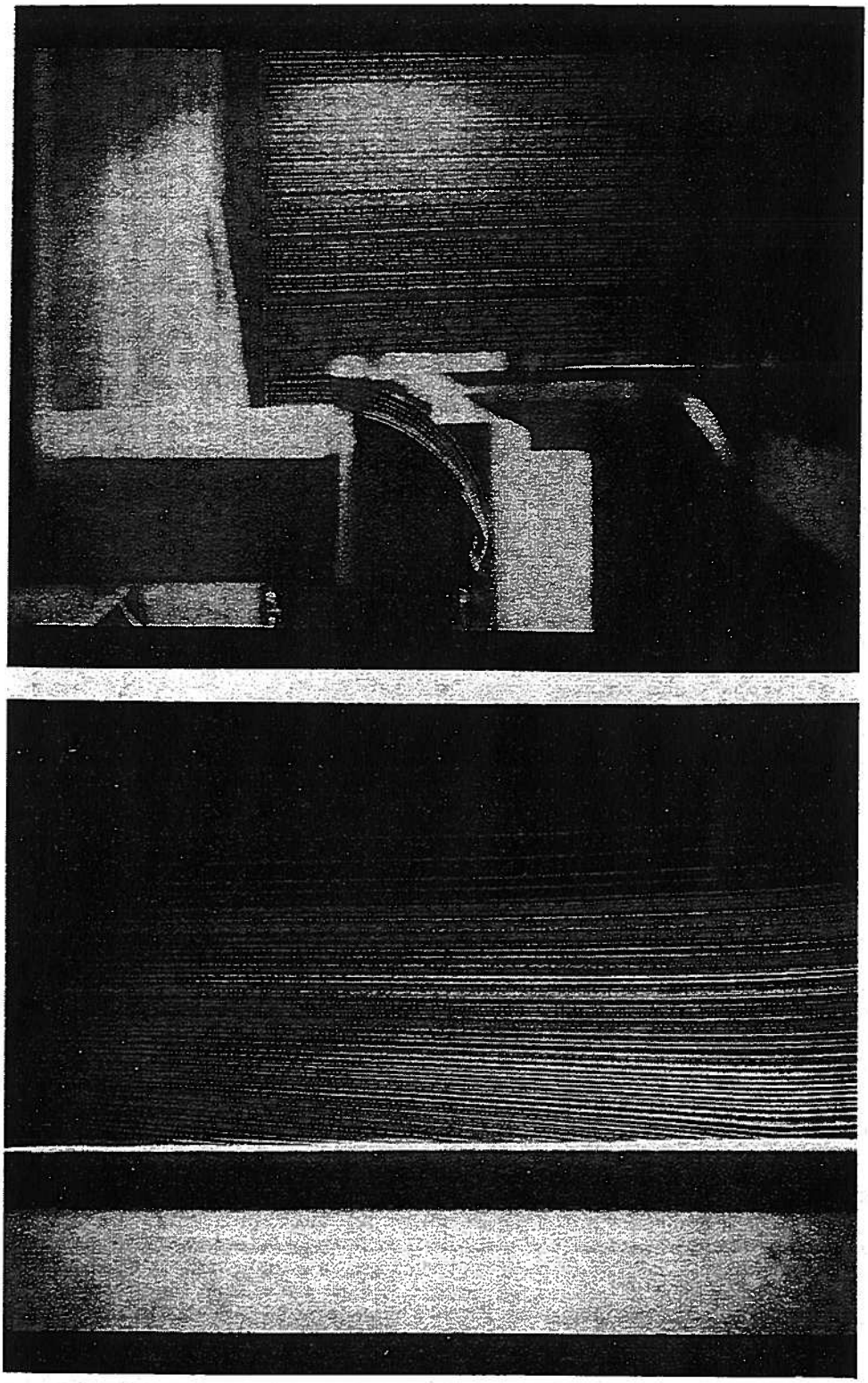

Fig. 3 Side view of smoke wire results for 1 m/s wind flow from left to right over a face-up horizontal absorber. Top: leading edge boundary layer removal. Bottom: effect of suction mass flow rate = 0.10 kg/m²-s.

the three geometry parameters plus suction mass flow rate. When one of these parameters was found to have a low sensitivity (plate thickness), it was replaced first by wind speed and then by plate orientation (vertical versus horizontal) in additional factorial runs.

A series of eight original test plates were manufactured to perform the first full-factorial statistical experiment to determine the relative impact of varying hole size, spacing, and plate thickness over the ranges expected for transpired collector applications. A plot of all plate geometries (showing hole diameter and pitch, but not thickness) is shown in Fig. 5.

All plates were made of aluminum and painted on one side

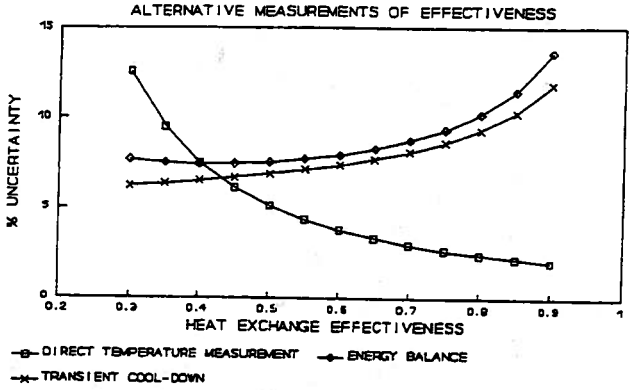

Fig. 4 Experimental uncertainty of effectiveness measurement versus effectiveness for three measurement methods

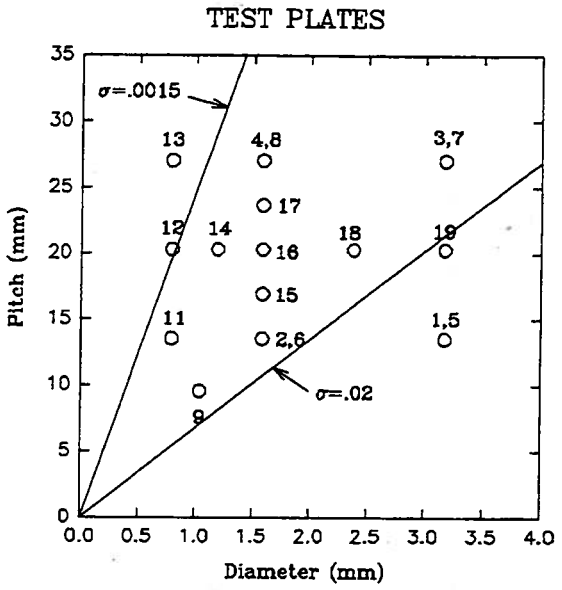

Fig. 5 Plot showing hole pitches and diameters for all test plates

with a flat black paint. Holes were then punched on a computer-controlled punching machine. The first eight test plates, numbers 1 through 8, form a cube in test space. (Note that plates 5, 6, 7, and 8 have the same hole diameters and pitches as plates 1, 2, 3, 4, respectively, but a different plate thickness. Plates 1–8 form a square in Fig. 5, since plate thickness is not plotted.)

Although the original test plates tend toward the high-porosity end of the range, this was necessary to meet the manufacturing constraint that hole diameter exceed plate thickness and still allow a 2 to 1 variation for hole diameter and for plate thickness. Plate 9 represents the geometry employed in a large outdoor test wall at NREL. The other plates were tested to provide additional data points for the correlation development.

The factorial tests revealed that the important parameters in determining heat exchange effectiveness are suction flow rate, wind speed, hole pitch, and hole diameter. Effectiveness increases with increasing wind speed and decreases with increasing suction flow rate, pitch, or diameter. For thin plates (1.588 mm [1/16 in.] or smaller), the actual plate thickness has a very small effect. The increase in effectiveness due to increasing plate thickness from 0.794 mm (1/32 in.) to 1.588 mm (1/16 in.) was only about 2 percent, or on the order of

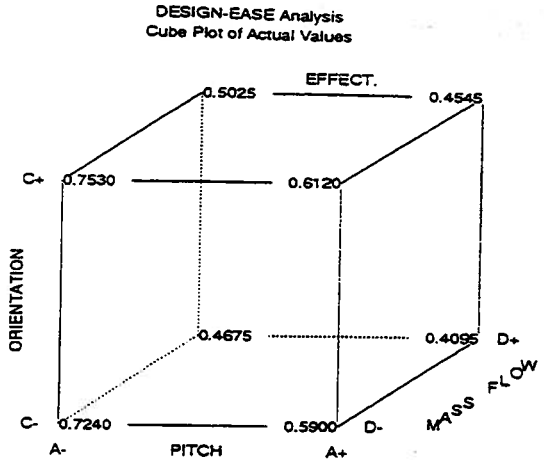

Fig. 6 Cube plot of measured effectiveness for investigation of orientation

the experimental uncertainty. Plate orientation (vertical versus horizontal) had only a slightly larger effect as shown in the cube plot of Fig. 6. As a result of the factorial experiments, it was decided to test all plates at a thickness of 1/32 in. (the thickness typically employed in the field) and in a vertical orientation, as this orientation gave a slightly higher value and is the typical orientation for solar ventilation preheat applications.

All of the plates shown in Fig. 5 were tested over a range of suction mass flow rate, G, from 0.02 to 0.07 kg/m^2-s. (At G values less than 0.02, the outlet temperature measurement became sensitive to the outlet probe locations, and at G values greater than 0.07, the uncertainty in ΔT measurement became too high due to the low value of ΔT.) For each case, the effectiveness was directly measured, and an overall U based on the front surface area (excluding hole area) and the overall log mean temperature difference was determined. This overall U is related to effectiveness as follows:

$$\epsilon_{HX} = 1 - e^{-\mathrm{NTU}} \tag{5}$$

where

$$\mathrm{NTU} = \frac{UA}{\dot{m}C_p} = \frac{UA}{GA'C_p} = \frac{A}{A'}\frac{U}{GC_p}$$

Since A is the plate surface area minus the hole area and A' is the total frontal area (including holes), the ratio A/A' can be expressed in terms of the porosity, $\sigma = 0.907\ (D/P)^2$, as:

$$\frac{A}{A'} = 1 - \sigma \tag{7}$$

Various areas on which to base U, and various length scales for both Nusselt number and Reynolds number were tried in developing a satisfactory nondimensional correlation. The general form that collapsed the data best is similar to that used by Andrews and Bazdidi-Tehrani (1989), except that in this case the U value used in the Nusselt number is based on the log mean temperature difference rather than the difference between plate temperature and ambient temperature. All fluid properties were assumed constant and were based on the inlet (ambient) temperature (typically 27°C), since the temperature rises were small, and since the ambient temperature will most readily be known by the designer.

The best fit correlation equation for normal flow is

$$\mathrm{Nu}_D = 2.75\left(\frac{P}{D}\right)^{-1.2}\mathrm{Re}_D^{0.43} \tag{8}$$

This fit, shown in Fig. 7, has a coefficient of determination,

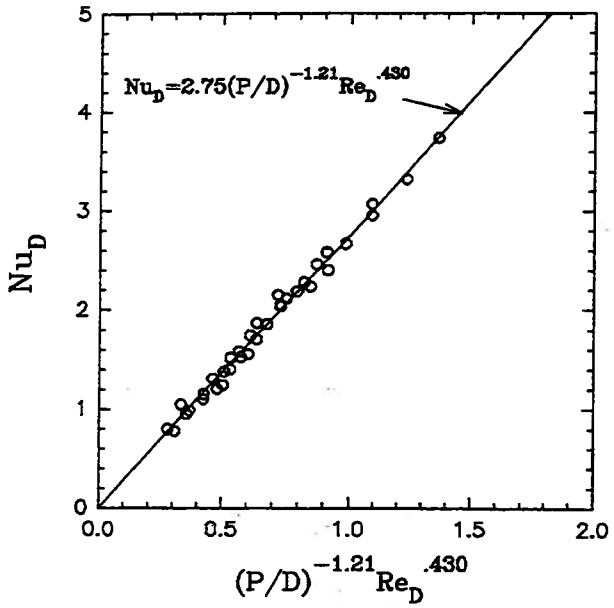

Fig. 7 Nu_D versus modified Re_D for vertical test plates

$Re \equiv V_{hole} D_{hole} / \nu$

R^2, of 0.990. The coefficients of variation of the three parameters are as follows:

Leading coefficient: 2.7 ± 6.8 percent

(P/D) exponent: -1.2 ± 1.9 percent

Re_D exponent: 0.43 ± 3.5 percent

It should be pointed out that since heat transfer occurs in three regions (front surface, hole, and back surface), there was no guarantee a priori that a single term correlation would provide a good fit for the overall heat transfer. Note that D is not the only possible selection of length scale. An algebraically equivalent correlation for normal flow in terms of pitch-based nondimensional parameters is:

$$Nu_p = 2.87\left(\frac{P}{D}\right)^{0.22} Re_p^{0.43} \tag{9}$$

but when the data are plotted in this form, they do not cluster as tightly.

5.0 Crosswind Effectiveness Results

As shown by Kutscher et al. (1993), for a flat plate in parallel flow with uniform suction, the theoretical starting length before the boundary layer reaches its final asymptotic state can be expressed as:

$$L_s \approx \frac{U_\infty \nu}{V^2} \tag{10}$$

Wind test data were taken under conditions in which the boundary layer could be considered at or very close to asymptotic. Suction mass flow rates were varied from 0.02 kg/m^2-s to a maximum of 0.07 kg/m^2-s, and the maximum wind speed tested was 4 m/s. The combination of minimum suction flow and maximum wind speed yields a maximum theoretical starting length of approximately 18 cm. This is based on a uniformly homogeneous suction surface and also does not account for the fact that a velocity boundary layer has already built up on a flat surface approximately 18–19 cm in length upstream of the absorber.

To test for the impact of downstream location, effectiveness measurements were taken both at the center of the absorber (25 cm downstream from the start of suction) and at a position 42 cm downstream from the start of suction. In each case, the local effectiveness was determined from measurements of the approaching air temperature (measured upstream from the absorber), the local surface temperature, and the local outlet temperature. It was found that the downstream measurement was always within 5 percent of the center plate measurement and usually much closer. Because results at the two locations were very close, and because the center location offered advantages such as direct comparison with zero-wind results (the same location and same surface and outlet sensors were used for the no-wind tests) and better isolation from plate edge losses, all of the wind results reported here are for the 25 cm location.

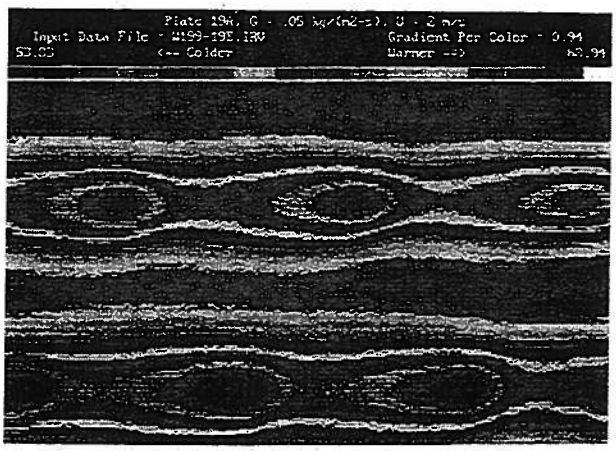

Fig. 8 Infrared image of black matboard absorber in WTS orientation; $G = 0.05$ kg/m^2-s, wind speed = 2 m/s (from right to left)

For a staggered array of holes on a triangular pitch, it is important to note that the geometry presented to the wind depends on the major direction. Consider orientation WTS (wide transverse spacing) as the one in which the spacing between holes measured in a direction transverse to the wind is wide and the NTS direction as the one in which this distance is narrow. The effect of orientation on front surface heat transfer was visualized using infrared thermography images. (The numerical results given by Kutscher, 1992, show that the heat transfer that occurs on the front surface dominates heat transfer in the hole and on the back surface at the geometries and suction flow rates of interest.) Absorbers made of black matboard were perforated with the same hole pattern as plate 19 and used for thermal visualization. These absorbers have low thermal conductivity and hence, with a constant surface heat flux, variations in local heat transfer coefficient are manifested as variations in the local temperature.

Figure 8 shows the surface temperature distribution for the WTS orientation with a suction mass flow rate of 0.05 kg/m^2-s and wind speed (from *right to left*) of 2 m/s. Surface temperatures are lowest near the edges of holes where acceleration of the flow thins the local boundary layer, thus raising the local heat transfer coefficient. Note that for this orientation, warm bands aligned in the flow direction exist between rows of holes.

Figure 9 shows the same suction and wind condition but for the NTS orientation. Note that the downstream banding that occurs in the WTS orientation does not occur in the NTS orientation.

Tests of two versions of several plates with both the WTS and NTS orientations of holes indicated that the NTS direction has a somewhat higher heat exchange effectiveness than the WTS direction. This is shown in Fig. 10 for plate 15. The upper two curves show effectiveness versus wind speed for a suction mass flow rate of 0.02 kg/m^2-s, while the lower curves are for $G = 0.07$ kg/m^2-s.

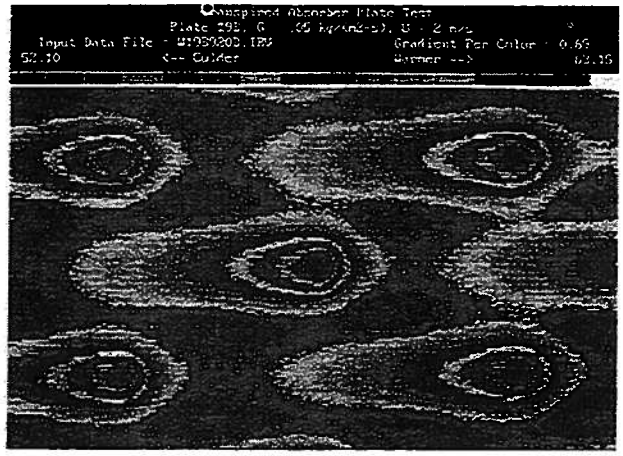

Fig. 9 Infrared image of black matboard absorber in NTS orientation; $G = 0.05$ kg/m^2-s, wind speed = 2 m/s (from right to left)

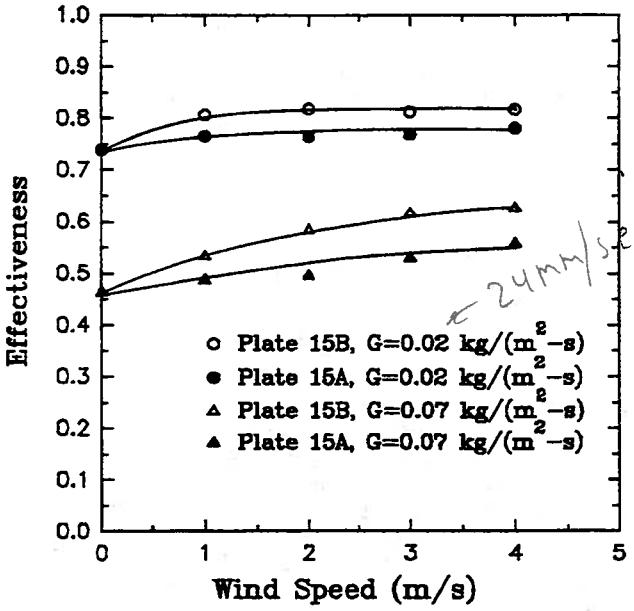

Fig. 10 Effect of hole orientation on wind test results. *A* denotes wide transverse spacing of holes and *B* denotes narrow transverse spacing

At each suction mass flow rate, a higher effectiveness is obtained for the NTS orientation of holes as compared with the WTS orientation. Because the higher performing orientation is of greater interest (one generally wants to maximize heat transfer), tests were run for seven different NTS orientation plates at all permutations of three suction mass flow rates ranging from $G = 0.02$ to $G = 0.07$ kg/m^2-s and at least three wind speeds (1, 2, and 4 m/s).

In seeking correlations for the wind results, it was found that at each individual wind speed, an accurate correlation could be obtained of the general form used for zero wind speed but with different values of coefficient and exponents. Various means were attempted for correlating all of the results into a single equation. The goal was to obtain a nondimensional correlation that reduced to the zero-wind case at zero wind and is zero at zero suction velocity. It appears reasonable to nondimensionalize the wind speed by dividing by the suction face velocity, V. This is because the asymptotic thermal boundary layer thickness is proportional to ν/V. Consider that the incremental heat transfer above the zero-wind value can be correlated in a form that relates a Nusselt number based on thermal boundary layer thickness to a Reynolds number based on the same length scale (and using wind speed as the velocity scale). Thus,

$$\mathrm{Nu}_\delta \sim \mathrm{Re}_\delta^x \tag{11}$$

Here the Nusselt number is based on an incremental heat transfer coefficient, $U' = U - U_0$, where U_0 is the value at zero wind and U is the value with nonzero wind. In terms of U' and δ,

$$\frac{U'\delta}{k} \sim \left(\frac{U_\infty \delta}{\nu}\right)^x \tag{12}$$

Noting that

$$\delta \sim \frac{\nu}{V} \tag{13}$$

the incremental heat transfer coefficient is:

$$U' \sim \frac{k}{\nu} V \left(\frac{U_\infty}{V}\right)^x \tag{14}$$

Note that if the exponent x is less than one, the incremental heat transfer coefficient goes to zero if wind speed or suction velocity go to zero.

Since the zero wind correlation is in the form of a Nusselt number based on hole diameter, it is convenient to multiply both sides of this equation by D/k, obtaining:

$$\mathrm{Nu}_D' \sim \sigma \mathrm{Re}_D \left(\frac{U_\infty}{V}\right)^x \tag{15}$$

and

$$\mathrm{Nu}_D = (\mathrm{Nu}_D)_0 + \mathrm{Nu}_D' \tag{16}$$

The wind data were thus fitted to a correlation of the form

$$\mathrm{Nu}_D' = a\sigma \mathrm{Re}_D \left(\frac{U_\infty}{V}\right)^b \tag{17}$$

Regression yielded:

$a = 0.0305$

$b = 0.48$

The coefficients of variation were ± 18.3 percent for a and ± 9.3 percent for b.

Thus the crosswind data for the narrow transverse spacing (NTS) were correlated as:

$$\mathrm{Nu}_D = 2.75\left[\left(\frac{P}{D}\right)^{-1.2} \mathrm{Re}_D^{0.43} + 0.011\sigma \mathrm{Re}_D \left(\frac{U_\infty}{V}\right)^{0.48}\right] \tag{18}$$

Note that for laminar flow over a plate, one expects an exponent on the wind speed of 1/2, and the fitted exponent is close to that. A plot of Nu_D for the nonzero wind data is shown in Fig. 11. When this correlation is used to determine heat exchange effectiveness, all measured heat exchange effectiveness values for the wind runs are predicted to within ± 9 percent. The R^2 value for predicted versus measured effectiveness for wind runs was 0.926.

6.0 Pressure Drop

In the design of a transpired collector, it is necessary to know heat exchange effectiveness to determine thermal performance. It is also necessary to predict pressure drop to ensure that it is sufficient to provide good flow uniformity and prevent outflow and in order to minimize fan power. The most comprehensive source that could be found on pressure drop information is the Russian work edited by I. E. Idelchik, entitled *Handbook of Hydraulic Resistance* (Idelchik, 1986).

Data for the Reynolds number (based on hole diameter) range of interest (about 100 to 2000) are given on p. 406 of that book in the form of graphs and tables for a wide porosity range, but are stated as "tentative" for this flow regime. De-

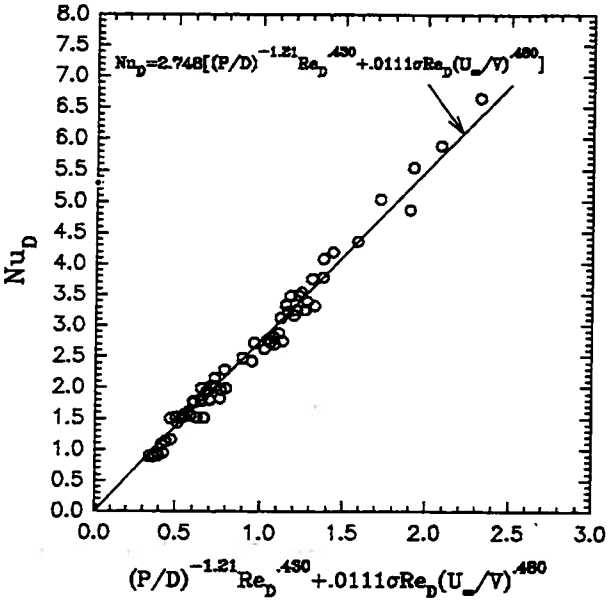

Fig. 11 General heat transfer correlation for nonzero wind tests

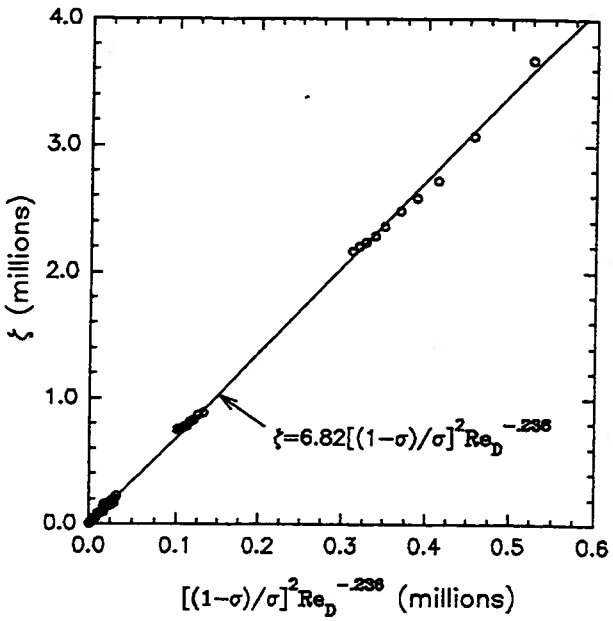

Fig. 12 Data and correlation for nondimensional pressure drop as a function of porosity and Reynolds number

termining the pressure drop for any given plate requires a complicated series of steps to evaluate various parameters and combine them into a final result.

In order to test the validity of the Idelchik data and to explore the possibility of a simpler correlation, all plates of 0.794 mm (1/32 in.) thickness were tested at suction mass flow rates from 0.01 to 0.08 kg/m^2-s. (Only data points with a minimum pressure drop of 5 Pa were recorded.) Flow rate was measured with the laminar flow element, and pressure drop was recorded by reading a Dwyer point gage manometer. This manometer has a range of 0-498 Pa (0-2 in. of water) and is readable to 2.29 Pa (0.001 in.).

The mean of the absolute value of the percentage error between the measured value and that calculated from the handbook was 14.6 percent with the highest error being 44 percent. Clearly there was room for improvement in predicting the pressure drop for these low-porosity plates.

The nondimensionalized pressure drop, ζ, is defined as:

$$\zeta \equiv \frac{\Delta P}{\frac{1}{2}\rho V^2} \tag{19}$$

where V is the approaching face velocity. An uncertainty analysis indicated that the nondimensionalized pressure drop could be measured with an overall experimental accuracy of ±6 percent. According to Idelchik (1986), ζ is a function of porosity, the Reynolds number based on hole diameter, and the friction factor. In seeking a simple single-term correlation for ζ, one can thus simply consider products of porosity and Reynolds number to unknown powers. In order not to prejudice the correlation, however, curve fits were done to determine dimensional pressure drop in terms of powers of hole pitch, hole diameter, and approach velocity. The resulting powers were highly consistent with the nondimensional variables given above.

When fitting the nondimensional variables, the power on porosity was very close to -2, that is, ζ was approximately proportional to $1/\sigma^2$. As shown by Batchelor (1967), the pressure drop across a perforated plate is analogous to a sudden enlargement in a pipe, and the decrease in the Bernoulli constant (i.e., the unrecoverable pressure drop) can be determined in nondimensional form from conservation of momentum as:

$$\zeta = \left(\frac{1-\sigma}{\sigma}\right)^2 \tag{20}$$

Batchelor points out that viscosity is not important unless the holes are very small. Note that for the plates tested here, which have very low porosity,

$$\left(\frac{1-\sigma}{\sigma}\right)^2 \approx \frac{1}{\sigma^2} \tag{21}$$

so that it is not surprising that the data show an inverse dependence on the square of the porosity.

Expressing the porosity term in Batchelor's form is consistent with the physics and could be expected to make the correlation more extrapolatable to higher porosities. Because it did not decrease the accuracy of the fit, this term was used in the correlation. The fact that the curve fitting yields a nonzero exponent on the Reynolds number indicates that the holes are small enough for viscosity to play a role in the pressure drop. The best fit for normal flow pressure drop for the plates tested was:

$$\zeta = 6.82\left(\frac{1-\sigma}{\sigma}\right)^2 Re_D^{-0.236} \tag{22}$$

When compared with the data, this fit yields an average value for the absolute magnitude of the error equal to 6.5 percent, but with a few considerably higher errors, the extreme being 26 percent. The coefficient of determination, R^2, for the fit is 0.9992. Thus this simple correlation fits the data better than the much more complicated procedure presented by Idelchik (1986). In fairness to Idelchik, the correlation presented here covers a much smaller range, namely the range suitable for transpired solar collectors. The correlation results together with the data are presented in Fig. 12.

All of the above-mentioned data were taken in the absence of a crosswind. A few runs were made to test the effect of a crossflow, and it was found that wind increases the pressure drop a small but significant amount. This can be seen in Fig. 13, which shows the increase in pressure drop for plate 17 as a function wind speed. Tests with both the WTS and NTS orientations showed no measurable effect of hole orientation on pressure drop.

Numerical analysis (Kutscher, 1992) shows that a separation

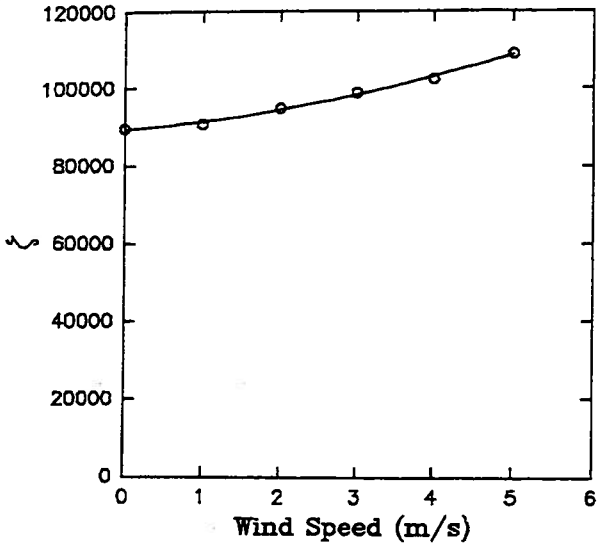

Fig. 13 Nondimensional pressure drop versus wind speed at $G = 0.023$ kg/m^2-s for plate 17

region occurs in the hole, and this likely has the effect of decreasing the effective hole size, thereby increasing the magnitude of the sudden enlargement. A detailed study of the effect of wind on pressure drop was beyond the scope of this study.

7.0 Summary and Conclusions

Perforated plates used for new solar collector applications are of low porosity and utilize very low flow rates at which the heat exchange effectiveness approaches its theoretical limit of one. In order to calculate the efficiency of such a device, the heat exchange effectiveness for the suction air stream must be known. This study showed that satisfactory heat transfer correlations can be developed if one defines an overall heat transfer coefficient based on the non-hole upstream surface area and the log mean temperature difference. It was shown that the major factors affecting heat transfer are suction flow rate, crosswind speed, hole pitch, and hole diameter. For thin plates, the actual thickness has little impact. Also, the enhancement associated with a vertical orientation as opposed to a horizontal orientation is slight. In the presence of a crosswind, the major orientation of the holes is important, with higher effectiveness values obtained in the case of the orientation with a lesser spacing in the cross-stream direction of hole rows. For plate porosities of 0.1 to 5 percent and hole Reynolds numbers of 100 to 2000, the following correlation for Nusselt number (for the narrow transverse hole spacing) predicts heat exchange effectiveness values to within ±9 percent:

$$\mathrm{Nu}_D = 2.75\left[\left(\frac{P}{D}\right)^{-1.2}\mathrm{Re}_D^{0.43} + 0.011\sigma\,\mathrm{Re}_D\left(\frac{U_\infty}{V}\right)^{0.48}\right] \quad (23)$$

Note that this correlation, even with U_∞ set to zero, cannot be directly compared with the results of Andrews and Bazdidi-Tehrani, since the correlation here is based on the log mean temperature difference, a necessity for the flow rate range for which this correlation is intended.

For plate porosities of 0.1 to 2.2 percent and hole Reynolds numbers of 100 to 2000, the following simple correlation for nondimensional pressure drop for normal flow yields an average error of 6.5 percent (but with some errors as high as 26 percent):

$$\zeta = 6.82\left(\frac{1-\sigma}{\sigma}\right)^2 \mathrm{Re}_D^{-0.24} \quad (24)$$

Acknowledgments

The author gratefully acknowledges the assistance provided by H. Doug Powell, Keith Gawlik, and Mark Lichtwardt at NREL, the advice given by Dr. John Daily of the University of Colorado at Boulder, and the financial support provided by Bob Hassett of the U.S. Department of Energy.

References

Andrews, G. E., and Bazdidi-Tehrani, F., 1989, "Small Diameter Film Cooling Hole Heat Transfer: The Influence of the Number of Holes," ASME Paper No. 89-GT-7.

ANSI/ASME PTC 19.1-1985, "ASME Performance Test Codes—Supplement on Instruments and Apparatus, Part 1: Measurement Uncertainty," American Society of Mechanical Engineers.

Batchelor, G. K., 1967, *An Introduction to Fluid Dynamics*, Cambridge University Press, Cambridge, United Kingdom.

Idelchik, I. E., 1986, *Handbook of Hydraulic Resistance*, Hemisphere Publishing Company, New York.

Kutscher, C. F., 1992, "An Investigation of Heat Transfer for Air Flow Through Low-Porosity Perforated Plates," Ph.D. thesis, Department of Mechanical Engineering, University of Colorado, Boulder, CO, Dec.

Kutscher, C. F., Christensen, C. B., and Barker, G. M., 1993, "Unglazed Transpired Solar Collectors: Heat Loss Theory," ASME *Journal of Solar Energy Engineering*, Vol. 115, pp. 182–188.

Sparrow, E. M., and Ortiz, M. C., 1982, "Heat Transfer Coefficients for the Upstream Face of a Perforated Plate Positioned Normal to an Oncoming Flow," *International Journal of Heat and Mass Transfer*, Vol. 25, No. 1, pp. 127–135.